PCCP

COMMUNICATION

View Article Online
View Journal | View Issue

Cite this: *Phys. Chem. Chem. Phys.*, 2017, **19**, 8661

Received 10th December 2016,
Accepted 28th February 2017

DOI: 10.1039/c6cp08450h

rsc.li/pccp

Water and hexane in an ionic liquid: computational evidence of association under high pressure†

A. Mariani,[a] R. Caminiti[ab] and L. Gontrani*[a]

High pressures may strongly affect the mesoscopic structure of some ionic liquids. In particular, the so called sponge-like structure is gradually destroyed when an increasing pressure is applied. Here we show how a polar solute, an apolar solute or a mixture thereof behave in the ionic liquid trihexyl, tetradecylphosphonium bis (trifluoromethylsulfonyl) imide when the pressure is raised up to 10 kbar. Our calculations clearly show an association between molecules that would not interact in ordinary conditions.

While the studies on ionic liquids (ILs) are widely diffused nowadays,[1–6] only in recent years is the attention being shifted to the mixtures of these compounds.[7–20] Their properties as solvents are so great to the extent that some of them could replace common organic solvents.[21,22] ILs are often called "Task Specific Solvents"[23–25] due to the exceptional tunability of their chemical and physical properties by even small changes in the molecular structure.[26] Most of the solvent behaviour of ILs arises from their characteristic mesoscopic structure, which is made up of a distorted polar domain percolating through an apolar domain, resembling a sponge.[27–33] This particular arrangement is responsible for the so-called Low q Peak (LqP) in the Small Angle X-ray Scattering (SAXS) pattern of such compounds.[34,35]

Recently, it has been established both experimentally[36] and computationally,[37–40] that by applying a high pressure to some ILs the LqP almost vanishes resulting in a homogenization of the system. The proposed model of folding alkyl tail(s) is based on the observation that ILs containing polar substituents on the chain(s) do not show the LqP – and, consequently, the domain segregation – because the tail tends to interact with the charged head folding on itself.[33] The same happens with alkyl chains stressed by pressure. The first and, as far as we know, unique experimental evidence for this effect was given by Yoshimura *et al.*[36] who reported vanishing of the LqP under pressure for 1-octyl-3-methylimidazolium tetrafluoroborate. Russina *et al.*[37] explained this observation using classical molecular dynamics suggesting the chain-folding model. A strong support for this rationalization was given by us in a recent study where we observed the same effect for short-chained protic ionic liquids[38] and *n*-alcohols[41] with alkyl chains containing 3 to 8 carbon atoms (Fig. 1 and 2).

Sharma *et al.* simulated some pyrrolidinium[39] and trihexyl, tetradecylphosphonium[40] ($P_{6,6,6,14}$) ILs giving a nice insight into the pressure effect. They stated that not only polar correlation but also charge–charge ordering is affected by compression. Another interesting result from the same group is the observation of an induced crystalline order at pressures higher than 2 kbar for $P_{6,6,6,14}$ bromide and $P_{6,6,6,14}$ dicyanamide. Here we want to answer the questions "*What happens to a solute accommodated in the (a)polar domain when such a domain is stressed by pressure?*" and "*What happens to two different solutes, one accommodated in the polar domain and the other in the apolar domain when the pressure is increased?*". To do so, we chose the ionic liquid $P_{6,6,6,14}$ Tf_2N (trihexyltetradecylphosphonium bis-(trifluoromethylsulfonyl)amide) because it can dissolve both small amounts of water – up to 0.087 water molar fraction[42] – and large

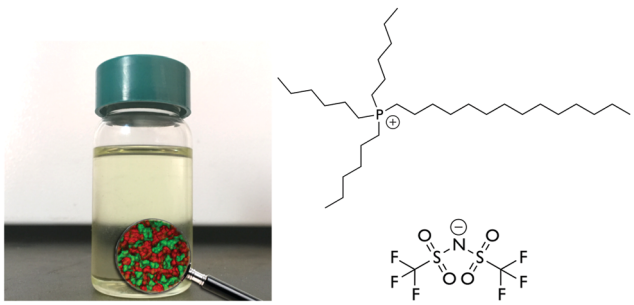

Fig. 1 (left) Representation of the sponge-like structure of some ionic liquids. Polar domain (red); apolar domain (green). (right)$P_{6,6,6,14}$ Tf_2N.

[a] *Department of Chemistry, "La Sapienza" University of Rome, P.le Aldo Moro 5, 00185 Rome, Italy. E-mail: alessandro.mariani@uniroma1.it, ruggero.caminiti@uniroma1.it, lorenzo.gontrani@uniroma1.it*

[b] *Centro di Ricerca per le Nanotecnologie Applicate all'Ingegneria, Laboratorio per le Nanotecnologie e le Nanoscienze, "La Sapienza" University of Rome, P.e Aldo Moro 5, 00185 Rome, Italy*

† Electronic supplementary information (ESI) available. See DOI: 10.1039/c6cp08450h

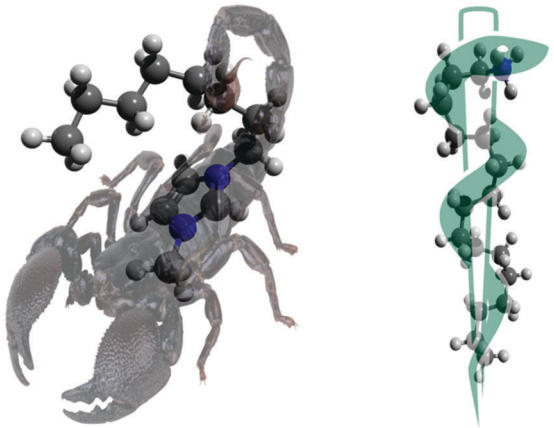

Fig. 2 *Scorpion* model (left) and *Asclepius* model (right)

quantities of hexane.[43] These two molecules are the perfect prototype for polar and apolar solutes respectively. As the state of the art suggests,[44,45] a series of different classical molecular dynamics simulations were carried out on four different systems: neat $P_{6,6,6,14}$ Tf_2N (PTF), $P_{6,6,6,14}$ Tf_2N saturated with water (PWA), $P_{6,6,6,14}$ Tf_2N with hexane (PHE), and $P_{6,6,6,14}$ Tf_2N with hexane and saturated with water (PWH). For each system, three different pressures were considered: 1 bar, 5 kbar and 10 kbar. The resulting SAXS patterns are shown in Fig. 3.

In the left panel of Fig. 3 the region in the q range 0.15–3.0 $Å^{-1}$ is reported. Regardless of pressure and/or composition changes, three peaks are always recognisable. Castner[46–48] and others[49,50] usually name these features after the correlation that generates them, so the LqP is called the polarity peak, the one at $\sim$0.7 $Å^{-1}$ the charge peak and the main peak is often referred to as the adjacency peak. Unlike the previously reported dialkyl-imidazolium,[36,37] dialkyl-pyrrolidinium[39] and alkyl-ammonium[38] ILs, the pressure appears to be unable to completely wear down the LqP, albeit it is strongly affected by compression. All the three features in PTF are lowered in intensity and shifted to higher q values, suggesting an overall loss of order and the shortening of the corresponding characteristic correlation length. The box snapshots for the neat IL clearly show a loss of the polar domain correlation as the pressure is raised, as can be seen in Fig. S1 of the ESI.† On the other hand, the apolar domain is almost unperturbed by pressure, probably because the cation $P_{6,6,6,14}$ induces a strong structuring. When hexane is added to the IL, the LqP appears to be sharper, suggesting that hexane further boosts such assembly, probably enhancing the aliphatic interactions between the cation chains, with the final result of a better defined apolar domain. Applying pressure to this mixture results in a behaviour not different from neat $P_{6,6,6,14}$ Tf_2N. The addition of water in PWA increases the shoulder on the left side of the LqP (highlighted in the right panel of Fig. 3), without affecting the other features. Interestingly, in PWH it is not possible to observe such a shoulder, but the LqP appears to be sharpened and shifted to smaller q values. So the overall change in PWH is a summation of the sharpening of the LqP by hexane and shifting of a LqP component to smaller q values by water, but in this case the shoulder is not resolved. Once compressed, PWA acts as a neat $P_{6,6,6,14}$ Tf_2N, but the shoulder on the left of LqP is always enhanced with respect to PTF. To better understand which correlations contribute to each peak, we have computed the following partial $S(q)$ for PWA, PHE and PWH: $S(q)_{cation-cation}$, $S(q)_{anion-cation}$, $S(q)_{anion-anion}$, $S(q)_{water-water}$, $S(q)_{water-hexane}$, $S(q)_{hexane-hexane}$, $S(q)_{CF_3}$. Results are shown in Fig. 4 and Fig. S2 in ESI.†

Like for other ILs,[51,52] the LqP is almost entirely due to anion–anion correlation, mediated by the cation size. The shoulder on the left side of the LqP is clearly visible also in the $S(q)_{anion-anion}$, but when hexane is added to the system, this feature is strongly decreased in intensity. The main contribution to that peak arises from the fluorinated domain as can be seen in Fig. S2 of the ESI.† Albeit in that figure a peak at $\sim$0.3 $Å^{-1}$ is always observable in $S(q)_{CF_3}$, it is increased in intensity and shifted to smaller q values in PWA, thus determining the resolution of the shoulder.

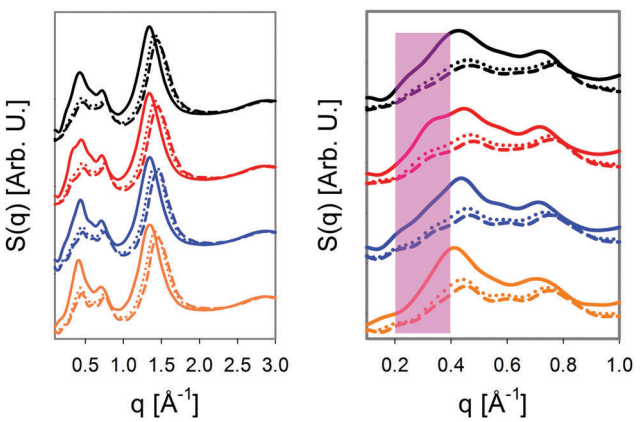

Fig. 3 Computational SAXS pattern of the systems studied. PTF (black); PWA (red); PHE (blue); PWH (orange). 1 bar (solid line); 5 kbar (dotted); 10 kbar (dashed).

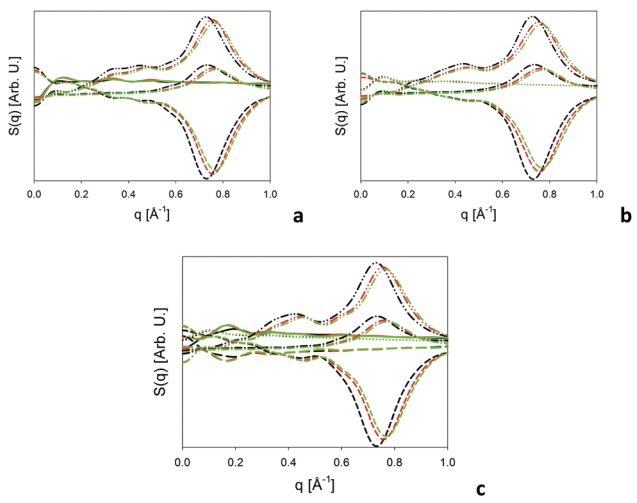

Fig. 4 Partial $S(q)$ for the systems studied. Cation–cation (dashed–dotted); anion–anion (dashed–double dotted); cation–anion (short dashed); water–water (solid); hexane–hexane (dotted); water–hexane (dashed). 1 bar (black); 5 kbar (red); 10 kbar (green). (a) PWA; (b) PHE; (c) PWH.

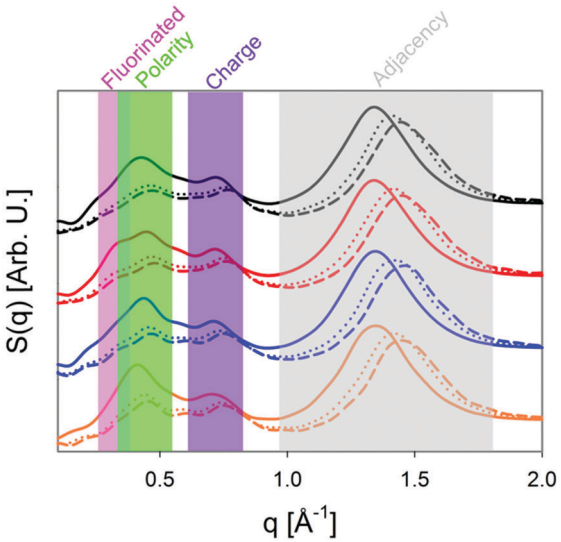

Fig. 5 Computed SAXS patterns for all the systems studied. The rectangles highlight the different regions of the patterns respect to the correlation which contributes to that peak. PTF (black); PWA (red); PHE (blue); PWH (orange). 1 bar (solid line); 5 kbar (dotted); 10 kbar (dashed).

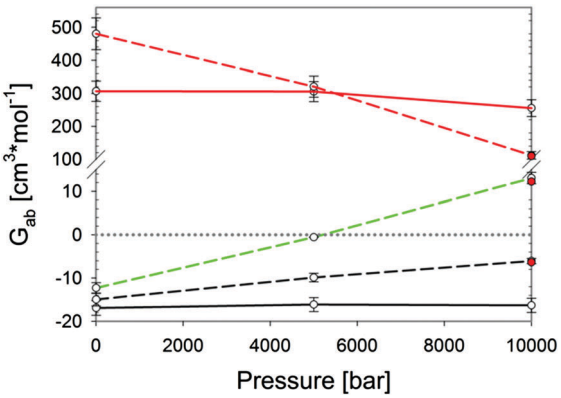

Fig. 6 Kirkwood Buff G_{ab} parameter for the system studied. Water–water (red); hexane–hexane (black); water–hexane (green). PWA (red, solid); PHE (black, solid); PWH (dashed). Red points refer to a simulation 100 ns long, made to check data reliability. The discrepancy between the values computed on the 5 ns trajectory and the ones obtained with the 100 ns one is negligible.

The existence of such a domain in certain ILs is a known fact,[53] but its fingerprint in the structure factor is often covered by the LqP. Moreover, the $S(q)_{\text{water–water}}$ shows a small peak in that region, enhancing the overall intensity. The consequent overall scenario is reported in Fig. 5. All the components show a linear dependence of both position and intensity with the applied pressure. The Kirkwood Buff theory (KB)[54,55] of solutions is a useful tool for quantifying molecular interactions, and, due to its sensitivity, KB may return quantitative results even if the relative quantity of a component is small, as in this case. The formula

$$G_{ab} = \int_0^{+\infty} [g_{ab}(r) - 1] \cdot 4\pi r^2 dr \quad (1)$$

where G_{ab} is the interaction parameter between a and b, $g_{ab}(r)$ is the pair distribution function of a and b, can return an overall picture of the molecular affinity. In Fig. 6 the G values obtained using (1) for the studied systems are shown.

At ambient pressure water appears to be strongly self-associated ($G \gg 0$), due to the strong hydrophobicity of $P_{6,6,6,14}$ Tf_2N. On the other hand, hexane is homogenously dispersed in the bulk ($G < 0$) thanks to the affinity with the long cation alkyl chains. $G_{\text{water–water}}$ appears to be much higher in PWH rather than PWA, this is due to the enhanced hydrophobicity induced by the hexane addition. $G_{\text{hexane–hexane}}$ is slightly less negative in PWH than PHE for the same reason, water has a repulsive effect on hexane and thus it is slightly less homogenous in PWH. When pressure in applied to the systems, $G_{\text{water–water}}$ and $G_{\text{hexane–hexane}}$ are almost unaffected in PWA and PHE respectively. In PWH, instead, the first has a drop of about 80% (400 cm^3 mol^{-1}) of its value at ambient pressure, and the second a rise of about 50% (7 cm^3 mol^{-1}). This means that the water clusters are widely destroyed, while hexane–hexane association is promoted.

The main result, though, is the trend of $G_{\text{water–hexane}}$. It has a negative value at ambient pressure (no interaction), almost a null value at 5 kbar and a positive value at 10 kbar (association). To further understand the water–hexane interaction, we checked the association in terms of cluster formation, just for the PWH system. The criteria for being part of a cluster are:

(i) A and B are in a cluster if at least one A atom is at a distance less than 4 Å from at least one B atom for at least 200 ps.

(ii) If A is in a cluster with B and B is in a cluster with C, then A, B and C are in the same cluster.

The results of the analysis are reported here in Fig. 7 and Table S2 in the ESI.†

The values on the x axes in Fig. 7 indicate how many atoms belong to a given cluster, *i.e.* an absolute value of 3 means the presence of a water molecule, while an absolute value of 20 means a hexane molecule. Consequently, the values in Fig. 3 and Table S2 (ESI†) should be read following the formula:

$$x = 3 \cdot N_{\text{water}} + 20 \cdot N_{\text{hexane}} \quad (2)$$

where N_{water} and N_{hexane} are the number of water and hexane molecules, respectively. The homomolecular interactions always decrease as pressure is raised while heteromolecular clusters appear to be much more prominent, especially $Water_2 \cdot Hexane_2$, $Water \cdot Hexane_3$, $Water \cdot Hexane_4$ and $Water_2 \cdot Hexane_4$. Therefore, it is evident how the pressure rise induces association between water and hexane, resulting in a forced hydration of the alkane. Summarising, our simulations highlighted how the IL meso-structure is deeply changed when compressing the system up to 10 kbar, in particular we focused on how the domain segregation is less pronounced. We checked four different systems, namely pure $P_{6,6,6,14}$ Tf_2N, its binary mixtures with water or hexane and the ternary system made up from them. In the simulations of all the systems at pressures up to 10 kbar we observed some interesting facts. The addition of water in PWA resulted in an enhanced structuration of the fluorinated domain, induced by the change in the conformational equilibrium of

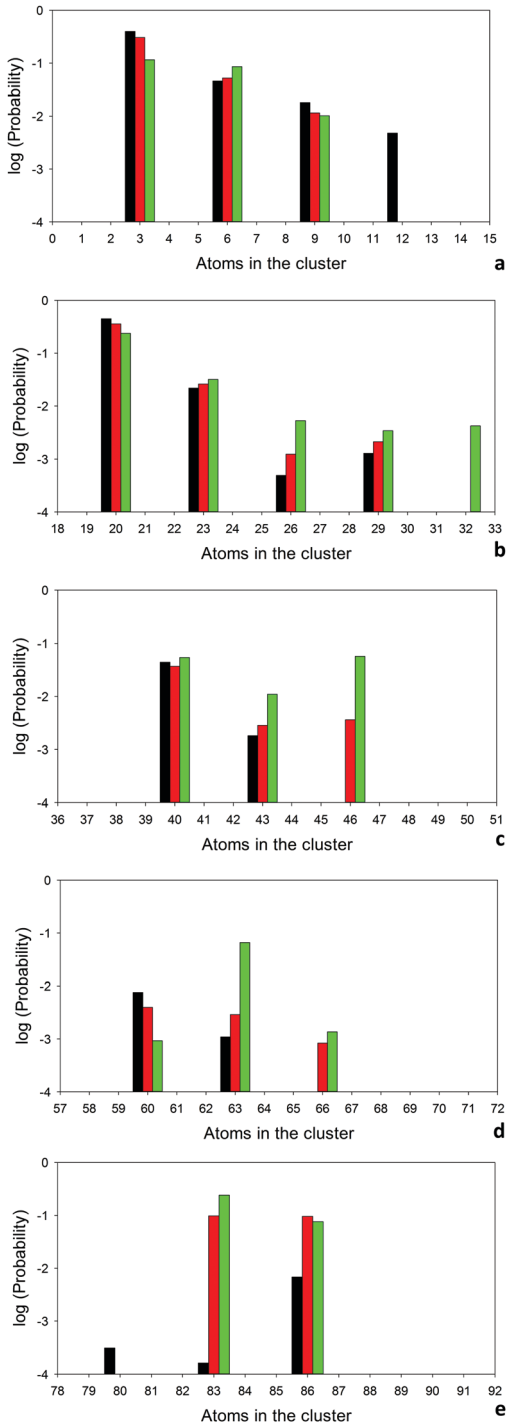

Fig. 7 Cluster analysis for the studied systems. 1 bar (black); 5 kbar (red); 10 kbar (green).

the anion, passing from ~22% *cis* (in good agreement with the literature[56]) to ~9% *cis*, as can be seen from the pair distribution function in Fig. S3 in the ESI.† This induced structuration is persistent upon application of pressure; nevertheless most of the mesoscopic organization is lost at 10 kbar. The same is true for PHE, where though hexane induces more structuration, upon compression the LqP is lowered in intensity and shifted to higher values. Finally, we clearly observed association between water and hexane mediated by the ionic liquid $P_{6,6,6,14}$ Tf_2N and induced by pressure rise in the ternary system PWH. This observation could foster new insights in the understanding of ILs properties and, perhaps more importantly, it could open up new synthesis routes and other applications for ILs.

Computational details

All the simulations were carried out using AMBER 14[57] with the GAFF force field.[58,59] For ionic species, the atomic charges were obtained by *ab initio* calculations at the B3LYP/6-311++G** level of theory using Gaussian09,[60] and applying the RESP algorithm.[61] Four different simulation boxes were prepared using PACKMOL.[62] Details of the boxes are in Table S1 in the ESI.† For each system, the following simulation route was applied:

10^7 minimization cycles; 500 ps *NVT* at 50 K; 10 ns *NPT* equilibration at 1 bar and 300 K; 10 ns *NVT* equilibration at 300 K; 5 ns *NVT* productive phase at 300 K; gradual pressure rising to 5 kbar using several 500 ps *NPT* simulations with incremental pressure (+200 bar for each step); 10 ns *NPT* equilibration at 5 kbar and 300 K; 10 ns *NVT* equilibration at 300 K; 5 ns *NVT* productive phase at 300 K; gradual pressure rising to 10 kbar using several 500 ps *NPT* simulations with incremental pressure (+200 bar for each step); 10 ns *NPT* equilibration at 10 kbar and 300 K; 10 ns *NVT* equilibration at 300 K; 5 ns *NVT* productive phase at 300 K. Each phase had a time step of 2 fs and the SHAKE algorithm was active. The trajectories of the productive phases were saved every 500 steps. The structure functions were computed using our standard procedure.[63] The cluster analysis was carried out with the utility clustsize of GROMACS[64] package. To check the reliability of the simulations, we performed a 100 ns productive *NVT* phase for PWH at 10 kbar and we found no differences in the results obtained with the 5 ns simulations, excluding the obvious gain in the statistics. Moreover, the computed total $S(q)$ for the neat IL was compared with the experimental data from Castner *et al.* and a satisfactory agreement was observed.[43,47]

References

1 J. S. Wilkes, *Green Chem.*, 2002, **4**, 73–80.
2 R. D. Rogers and K. R. Seddon, *Science*, 2003, **302**, 792–793.
3 C. A. Angell, N. Byrne and J.-P. Belieres, *Acc. Chem. Res.*, 2007, **40**, 1228–1236.
4 N. V. Plechkova and K. R. Seddon, *Chem. Soc. Rev.*, 2008, **37**, 123–150.
5 J. Dupont, *Acc. Chem. Res.*, 2011, **44**, 1223–1231.
6 T. Greaves and C. J. Drummond, *Chem. Rev.*, 2015, **115**, 11379–11448.
7 P. M. Mancini, G. G. Fortunato and L. R. Vottero, *Phys. Chem. Liq.*, 2004, **42**, 625–632.
8 M. Deetlefs, C. Hardacre, M. Nieuwenhuyzen, O. Sheppard and A. K. Soper, *J. Phys. Chem. B*, 2005, **109**, 1593–1598.
9 A. Jarosik, S. R. Krajewski, A. Lewandowski and P. Radzimski, *J. Mol. Liq.*, 2006, **123**, 43–50.

10 A. A. H. Pádua, M. F. Costa Gomes and J. N. A. Canongia Lopes, *Acc. Chem. Res.*, 2007, **40**, 1087–1096.
11 S. Thomaier and W. Kunz, *J. Mol. Liq.*, 2007, **130**, 104–107.
12 B. Fazio, A. Triolo and G. Di Marco, *J. Raman Spectrosc.*, 2008, **39**, 233–237.
13 Y. Kohno and H. Ohno, *Chem. Commun.*, 2012, **48**, 7119–7130.
14 R. Hayes, S. Imberti, G. G. Warr and R. Atkin, *Angew. Chem., Int. Ed.*, 2012, **51**, 7468–7471.
15 M. Piana, J. Wandt, S. Meini, I. Buchberger, N. Tsiouvaras and H. A. Gasteiger, *J. Electrochem. Soc.*, 2014, **161**, 1992–2001.
16 S. Omar, J. Lemus, E. Ruiz, V. R. Ferro, J. Ortega and J. Palomar, *J. Phys. Chem. B*, 2014, **118**, 2442–2450.
17 O. Russina, A. Sferrazza, R. Caminiti and A. Triolo, *J. Phys. Chem. Lett.*, 2014, **5**, 1738–1742.
18 O. Russina, A. Mariani, R. Caminiti and A. Triolo, *J. Solution Chem.*, 2015, **44**, 685–699.
19 A. Mariani, O. Russina, R. Caminiti and A. Triolo, *J. Mol. Liq.*, 2015, **212**, 947–956.
20 A. Mariani, R. Dattani, R. Caminiti and L. Gontrani, *J. Phys. Chem. B*, 2016, **120**, 10540–10546.
21 M. J. Earle and K. R. Seddon, *Pure Appl. Chem.*, 2000, **72**, 1391–1398.
22 N. Muhammad, Z. Man and M. A. Bustam Khalil, *Eur. J. Wood Wood Prod.*, 2011, **70**, 125–133.
23 A. E. Visser, R. P. Swatloski, W. M. Reichert, R. Mayton, S. Sheff, A. Wierzbicki, J. H. Davis and R. D. Rogers, *Environ. Sci. Technol.*, 2002, **36**, 2523–2529.
24 Z.-Z. Yang, Y.-N. Zhao and L.-N. He, *RSC Adv.*, 2011, **1**, 545.
25 C. Yue, D. Fang, L. Liu and T.-F. Yi, *J. Mol. Liq.*, 2011, **163**, 99–121.
26 R. Hayes, S. Imberti, G. G. Warr and R. Atkin, *J. Phys. Chem. C*, 2014, **118**, 13998–14008.
27 A. Triolo, O. Russina, H.-J. Bleif and E. Di Cola, *J. Phys. Chem. B*, 2007, **111**, 4641–4644.
28 A. Triolo, O. Russina, B. Fazio, G. B. Appetecchi, M. Carewska and S. Passerini, *J. Chem. Phys.*, 2009, **130**, 164521.
29 R. Atkin and G. G. Warr, *J. Phys. Chem. B*, 2008, **112**, 4164–4166.
30 R. Hayes, S. Imberti, G. G. Warr and R. Atkin, *Phys. Chem. Chem. Phys.*, 2011, **13**, 13544–13551.
31 R. Hayes, S. Imberti, G. G. Warr and R. Atkin, *Phys. Chem. Chem. Phys.*, 2011, **13**, 3237–3247.
32 O. Russina and A. Triolo, *Faraday Discuss.*, 2012, **154**, 97–109.
33 K. Shimizu, C. E. S. Bernardes, A. Triolo and J. N. Canongia Lopes, *Phys. Chem. Chem. Phys.*, 2013, **15**, 16256–16262.
34 O. Russina, A. Triolo, L. Gontrani and R. Caminiti, *J. Phys. Chem. Lett.*, 2012, **3**, 27–33.
35 O. Russina, W. Schröer and A. Triolo, *J. Mol. Liq.*, 2015, **210**, 161–163.
36 Y. Yoshimura, M. Shigemi, M. Takaku, M. Yamamura, T. Takekiyo, H. Abe, N. Hamaya, D. Wakabayashi, K. Nishida, N. Funamori, T. Sato and T. Kikegawa, *J. Phys. Chem. B*, 2015, **119**, 8146–8153.
37 O. Russina, F. Lo Celso and A. Triolo, *Phys. Chem. Chem. Phys.*, 2015, **17**, 29496–29500.
38 A. Mariani, R. Caminiti, M. Campetella and L. Gontrani, *Phys. Chem. Chem. Phys.*, 2016, **18**, 2297–2302.
39 S. Sharma, A. Gupta and H. K. Kashyap, *J. Phys. Chem. B*, 2016, **120**, 3206–3214.
40 S. Sharma, A. Gupta, D. Dhabal and H. K. Kashyap, *J. Chem. Phys.*, 2016, **145**, 134506.
41 A. Mariani, P. Ballirano, F. Angiolari, R. Caminiti, P. Ballirano, F. Angiolari, R. Caminiti and L. Gontrani, *ChemPhysChem*, 2016, **17**, 3023–3029.
42 M. Blesic, J. N. C. Lopes, M. F. C. Gomes and L. P. N. Rebelo, *Phys. Chem. Chem. Phys.*, 2010, **12**, 9685–9692.
43 M. Liang, S. Khatun and E. W. J. Castner, *J. Chem. Phys.*, 2015, **142**, 121101.
44 F. Dommert, K. Wendler, R. Berger, L. Delle Site and C. Holm, *ChemPhysChem*, 2012, **13**, 1625–1637.
45 L. M. Varela, T. Méndez-Morales, J. Carrete, V. Gómez-González, B. Docampo-Álvarez, L. J. Gallego, O. Cabeza and O. Russina, *J. Mol. Liq.*, 2015, **210**, 178–188.
46 E. W. Castner and J. F. Wishart, *J. Chem. Phys.*, 2010, **132**, 120901.
47 H. K. Kashyap, C. S. Santos, H. V. R. Annapureddy, N. S. Murthy, C. J. Margulis and E. W. J. Castner, *Faraday Discuss.*, 2012, **154**, 133–143.
48 H. K. Kashyap, C. S. Santos, N. S. Murthy, J. J. Hettige, K. Kerr, S. Ramati, J. Gwon, M. Gohdo, S. I. Lall-Ramnarine, J. F. Wishart, C. J. Margulis and E. W. Castner, *J. Phys. Chem. B*, 2013, **117**, 15328–15337.
49 S. Li, J. L. Bañuelos, J. Guo, L. Anovitz, G. Rother, R. W. Shaw, P. C. Hillesheim, S. Dai, G. a. Baker and P. T. Cummings, *J. Phys. Chem. Lett.*, 2012, **3**, 125–130.
50 J. C. Araque, J. J. Hettige and C. J. Margulis, *J. Phys. Chem. B*, 2015, **119**, 12727–12740.
51 M. Campetella, L. Gontrani, F. Leonelli, L. Bencivenni and R. Caminiti, *ChemPhysChem*, 2015, **16**, 197–203.
52 M. Campetella, D. C. Martino, E. Scarpellini and L. Gontrani, *Chem. Phys. Lett.*, 2016, **660**, 99–101.
53 O. Hollõczki, M. Macchiagodena, H. Weber, M. Thomas, M. Brehm, A. Stark, O. Russina, A. Triolo and B. Kirchner, *ChemPhysChem*, 2015, **16**, 3325–3333.
54 K. E. Newman, *Chem. Soc. Rev.*, 1994, **23**, 31.
55 P. E. Smith, *J. Chem. Phys.*, 2008, **129**, 1–6.
56 M. Deetlefs, C. Hardacre, M. Nieuwenhuyzen, A. a H. Padua, O. Sheppard and A. K. Soper, *J. Phys. Chem. B*, 2006, **110**, 12055–12061.
57 D. A. Case, T. E. Cheatham, T. Darden, H. Gohlke, R. Luo, K. M. Merz, A. Onufriev, C. Simmerling, B. Wang and R. J. Woods, *J. Comput. Chem.*, 2005, **26**, 1668–1688.
58 J. Wang, R. M. Wolf, J. W. Caldwell, P. A. Kollman and D. A. Case, *J. Comput. Chem.*, 2004, **25**, 1157–1174.
59 K. G. Sprenger, V. W. Jaeger and J. Pfaendtner, *J. Phys. Chem. B*, 2015, **119**, 5882–5895.
60 M. J. Frisch, G. W. Trucks, H. B. Schlegel, G. E. Scuseria, M. A. Robb, J. R. Cheeseman, G. Scalmani, V. Barone, B. Mennucci, G. A. Petersson, H. Nakatsuji, M. Caricato, X. Li, H. P. Hratchian, A. F. Izmaylov, J. Bloino, G. Zheng, J. L. Sonnenberg, M. Hada, M. Ehara, K. Toyota, R. Fukuda,

J. Hasegawa, M. Ishida, T. Nakajima, Y. Honda, O. Kitao, H. Nakai, T. Vreven, J. A. Montgomery, Jr., J. E. Peralta, F. Ogliaro, M. Bearpark, J. J. Heyd, E. Brothers, K. N. Kudin, V. N. Staroverov, T. Keith, R. Kobayashi, J. Normand, K. Raghavachari, A. Rendell, J. C. Burant, S. S. Iyengar, J. Tomasi, M. Cossi, N. Rega, J. M. Millam, M. Klene, J. E. Knox, J. B. Cross, V. Bakken, C. Adamo, J. Jaramillo, R. Gomperts, R. E. Stratmann, O. Yazyev, A. J. Austin, R. Cammi, C. Pomelli, J. W. Ochterski, R. L. Martin, K. Morokuma, V. G. Zakrzewski, G. A. Voth, P. Salvador, J. J. Dannenberg, S. Dapprich, A. D. Daniels, Ö. Farkas, J. B. Foresman, J. V. Ortiz, J. Cioslowski and D. J. Fox, *Gaussian 09, Revision D.01*, Gaussian, Inc., Wallingford CT, 2013.

61 F. Y. Dupradeau, A. Pigache, T. Zaffran, C. Savineau, R. Lelong, N. Grivel, W. Rosanski and P. Cieplak, *Phys. Chem. Chem. Phys.*, 2010, 7821–7839.

62 L. Martínez, R. Andrade, E. G. Birgin and J. M. Martínez, *J. Comput. Chem.*, 2009, **30**, 2157–2164.

63 L. Gontrani, O. Russina, F. C. Marincola and R. Caminiti, *J. Chem. Phys.*, 2009, **131**, 244503.

64 S. Pronk, S. Páll, R. Schulz, P. Larsson, P. Bjelkmar, R. Apostolov, M. R. Shirts, J. C. Smith, P. M. Kasson, D. Van Der Spoel, B. Hess and E. Lindahl, *Bioinformatics*, 2013, **29**, 845–854.

